Multi-Bead-and-Spring Model to Interpret Protein Detachment Studied by AFM Force Spectroscopy

Csilla Gergely,* Joseph Hemmerlé,* Pierre Schaaf,† J. K. Heinrich Hörber,‡ Jean-Claude Voegel,* and Bernard Senger*

*Institut National de la Santé et de la Recherche Médicale, Unité 424, UFR d'Odontologie, Université Louis Pasteur, 67085 Strasbourg Cedex, France; †Institut Charles Sadron, Centre National de la Recherche Scientifique, Université Louis Pasteur, 67083 Strasbourg Cedex, France; ‡European Molecular Biology Laboratory, 69012 Heidelberg, Germany

ABSTRACT This article deals with the detachment of molecules (fibrinogen) from a surface studied experimentally with an atomic force microscope. The detachment (or rupture) forces are measured as a function of the retraction velocity and exhibit a clear dependence on this parameter, even though the interaction between the molecules and the surface are nonspecific. To interpret these data, a mechanical multi-bead-and-spring model is developed. It consists of one to several parallel, "molecular" springs connected to an extra spring representing the cantilever that is moved at constant velocity. The free end of each molecular spring terminates with a particle that interacts with the surface through a Lennard-Jones potential. This Brownian dynamics model is used to analyze the experimental findings. In the framework of this model, it appears that the fibrinogen molecule must be ascribed a stiffness much smaller than that of the cantilever. In addition, several bonds between the molecule and the surface must be taken into account for the range of the molecule-surface interaction not to be unrealistically small. In future work, this model will be extended to more complex mechanisms such as the detachment of cells from a surface.

INTRODUCTION

Force spectroscopy is mostly used to determine the unbinding force between two molecules (e.g., a ligand/receptor couple) (Moy et al., 1994; Dammer et al., 1996; Hinterdorfer et al., 1996, 1998; Fritz et al., 1998; Willemsen et al., 1998; Fisher et al., 1999; Lo et al., 1999; Merkel et al., 1999; Rief et al., 1999; Strigl et al., 1999; Strunz et al., 1999, 2000) and more recently between two cells (Dufrêne et al., 1999; Benoit et al., 2000). In the present work, atomic force microscopy (AFM), which allows in principle very weak forces ($\geq$10 pN) to be measured (Hoh et al., 1992), has been applied to evaluate the force involved in the detachment of a protein (fibrinogen) adsorbed on a solid surface (silica and mica), a domain that seems to be investigated less frequently (Eckert et al., 1997; Bowen et al., 1998; Hemmerlé et al., 1999; Gergely et al., 2000, 2001). Whereas the first examples concern specific interactions, the adhesion of fibrinogen on a bare surface is nonspecific and can thus take place simultaneously on different locations of the molecule and of the surface. Despite this difference, the detachment of a molecule from a surface or from another molecule displays a universal feature: the rupture force measured using an AFM or the micropipette technique is not an intrinsic property of the interaction but depends on the loading rate R_f, i.e., on the increase of the pulling force per time unit, as recognized by Bell over 20 years ago (Bell, 1978; see also Evans and Ritchie, 1997; Evans, 1998, 1999; Strunz et al., 2000). A similar behavior is found for the detachment of cells from a surface (Bongrand, 1994; Mège et al., 1986). This can be viewed in the following simple picture: a bond is depicted as a particle located in a potential energy well resulting from, e.g., the electrostatic and van der Waals interactions between the molecule and the surface, whose deepest point is located near the surface, and which displays an increasing asymptotic branch. Such a bond cannot break because the particle cannot escape over an energy barrier that extends to infinity. In contrast, as soon as the bond is submitted to an external force, whether constant in time or not but independent of the location of the particle at a given time, the top of the energy barrier moves to a finite distance (see, e.g., Fig. 1 in Gergely et al., 2000). This introduces an objective subdivision of the space into a region where the molecule is attached (left hand side of the top of the barrier, also called transition state) and a region where it is detached (right hand side of the top of the barrier). However, in general, the bond between the particle and the surface is reversible, i.e., the particle can recross the top of the barrier toward the surface and rebind. As a consequence, the time elapsed until the last passage over the barrier, while the particle diffuses away from the surface, can be considerably larger than the first passage time over this barrier (Evans and Ritchie, 1997; Ritchie, 1998). This lengthening of the detachment time, observed when decreasing external forces are successively applied to the bond, has two origins: on the one hand, the first passage

Submitted December 13, 2001, and accepted for publication March 28, 2002.

Address reprint requests to Bernard Senger, Institut National de la Santé et de la Recherche Médicale, Unité 424, UFR d'Odontologie, Université Louis Pasteur, 11, rue Humann, 67085 Strasbourg Cedex, France. Tel.: 33-03-90-24-32-58; Fax: 33-03-90-24-33-79; E-mail: bernard.senger@medecine.u-strasbg.fr.

C. Gergely and J. Hemmerlé contributed equally to this work.

C. Gergely's permanent address is Institute of Biophysics, Biological Research Center, Hungarian Academy of Sciences, 6701 Szeged, Hungary.

0006-3495/02/08/706/17 $2.00

time increases and, on the other hand, the number of recrossings increases. Both effects co-operate to a protracted detachment time. This is a general law applying to the escape over an energy barrier under the sole action of the thermal energy transferred from the surrounding medium (the solvent) to the molecule. In particular, this is also true for a cell detaching from a surface, as suggested by Mège et al. (1986) who showed experimentally that cells adhering on glass resist a liquid flow (i.e., a shear stress) for a duration that decreases when the flow rate increases. The same qualitative behavior was observed by van Kooten et al. (1992) who showed, in addition, that the adhesion time of cells depends on the wettability of the substratum. In this case, as well as for a molecule, there is still a complicating factor. Indeed, there is no reason to state a priori that the adhesion either of a molecule or of a cell is described by a single bond. The detachment time of the whole molecule or cell becomes then the longest among the detachment times of the individual bonds. The reciprocal of the detachment time represents the off-rate $v(f)$ corresponding to a given pulling force f.

To get information on the rupture force one considers a molecule submitted to a pulling force whose strength increases with time, most often linearly, from zero on. Then, after each force increment, the energy barrier is lowered, and the escape probability increases accordingly. Such a linear increase of the force strength (at the rate equal by definition to $R_f = df/dt$) can in principle be achieved with an AFM where the adsorbing surface moves at constant velocity and bends the cantilever, which acts as a spring, linked to the surface by the molecule to be detached. In this way, the molecule is submitted to a linearly increasing force, $f = R_f t$, as long as thermal fluctuations do not appreciably perturb this relation, i.e., as long as R_f can reasonably be considered as independent of t. The applied force is continuously recorded so that, once the detachment is observed, the force exerted by the cantilever on the molecule, which leads to the break, is known and represents the rupture force. However, this latter depends on the loading rate as already evoked above: the larger the loading rate, the larger the rupture force, i.e., the external force that had to be applied to achieve the detachment. When R_f is small, the pulling force grows slowly, and the barrier height falls off slowly too. Then, the escape of the molecule occurs generally much before the barrier is eliminated, because the thermal energy supplied by the medium becomes sufficient for the molecule to diffuse over the lowered barrier. In contrast, when R_f is large, the pulling force grows rapidly and induces the elimination of the barrier before the thermal diffusion could be effective.

Bell (1978) stated that the off-rate $v(f)$ increases exponentially with f. One can then derive a relationship between the most probable rupture force (Evans and Ritchie, 1997) or the mean rupture force (Gergely et al., 2000) and the loading rate assumed to be constant. It has been shown that this exponential law corresponds to the particular case of a sharp barrier (Evans, 1999; Evans and Ludwig, 2000), which, strictly speaking, appears only when the potential energy increases linearly with the molecule-to-surface distance up to a point where it becomes zero and stays zero beyond. Under these circumstances, the top of the barrier does not move when f increases. As a consequence, the distance from the deepest point of the well to the top of the barrier, i.e., the width of the barrier, stays constant, and the barrier height decreases linearly with f. The argument of the exponential appearing in the expression for the off-rate is then also a linear function of f. However, there is no strong argument in favor of the representation of the adhesion of a molecule to a surface by such a peculiar potential energy well. For instance, if the van der Waals interaction is responsible for the attachment, the interaction intensity decays following an inverse power law of the distance, rather than linearly. In such a case, it can be verified that the barrier height is not a linear function of f. Furthermore, in the case of the AFM, the particle moves in an energy landscape that results from the addition of the surface potential energy and of the harmonic energy well due to the cantilever.

To overcome the difficulties raised by possible multiple interaction points and the nonvalidity of Bell's assumption, we propose a multi-"bead-and-spring" model to describe the detachment of proteins or cells from a surface by AFM type experiments. Our model is defined by n beads attached to n parallel springs (one bead per spring) themselves related to a transducer consisting of a spring, which serves to pull the system away from the surface under various loading rates. Each particle (i.e., bead) is assumed to interact with the substrate by a potential energy well whose main characteristics is to be attractive from a given distance on. Each bead-and-spring couple and its associated well may be thought as representing the internal elasticity of the molecule and the interaction of a group of atoms of this molecule with the surface. Each particle thus diffuses in a potential well and its movement is simulated using a Brownian dynamics algorithm. Our model accounts for the fact that a particle that has crossed the energy barrier can diffuse back over the barrier. This corresponds to a reversible bond, i.e., a bond that breaks and reforms for an unpredictable number of times. It takes also into account the fact that for a molecule or a cell to be detached from the surface all the bonds need to have crossed the energy barrier. Finally, the proposed simulation model avoids any assumption on the dependence of the off-rate $v(f)$ on the applied force. Repeating the simulation of the detachment process for a given loading rate permits the average rupture force to be determined, and using a large range of loading rates (covering several orders of magnitude) leads to the relationship between the mean rupture force and the loading rate. For illustration we shall apply our model to analyze the detach-

ment process of fibrinogen molecules adsorbed on silica and mica surfaces, investigated by AFM force spectroscopy.

The remaining of the paper is organized as follows. In the next section we summarize the materials and methods used for carrying out the experiments on the detachment of fibrinogen adsorbed on either a silica or a mica surface. Then, we describe the multi-bead-and-spring model. Its properties are first discussed in the particular case where the molecule is represented by a single spring. Afterward we compare the rupture forces derived from this simplified version of our model to their experimental counterparts. It will be shown that the simplest model (i.e., the 1-bead-and-spring model) is unable to reproduce the experimental findings unless attributing values, unrealistic from a physical point of view, to one of the adjusted parameters entering the model. As a consequence the experimental data are reanalyzed using several parallel springs to represent the molecule. It will be seen that at high retraction rates the multi-bead-and-spring model behaves as the mono-bead-and-spring model up to a scaling factor equal to the number n of springs. In contrast, at small loading rates, the results are not proportional to n. We shall show that the sensitivity of the rupture force to the loading rate decreases as the number of parallel springs increases. This is due to the fact that the modeled molecule behaves more and more as a macroscopic body when n increases, provided that the molecule is stiff compared with the cantilever. The multi-bead-and-spring model will serve in future work to model the detachment of adhering cells from surfaces. Finally, we give a summary and some concluding remarks.

MATERIALS AND METHODS

Atomic force microscope

Measurements were carried out with a specially designed AFM used in force-spectroscopy mode (Moy et al., 1994; Hemmerlé et al., 1999). In a force measurement, the sample is moved up and down by applying varying voltages to the piezoelectric translator onto which the sample is mounted while measuring the cantilever deflection. With our instrument it is possible to perform "approach/retraction" cycles in which the different cycle parameters (interaction time, approach, and retraction velocities) can be varied independently. In the new experiments shown here (mica surface), the approach rate and the interaction time were kept fixed: 900 nm s^{-1} and 1 s, respectively, whereas the retraction velocity v_r was varied in the range of 180 to 9×10^4 nm s^{-1}. In the former experiments (Gergely et al., 2000) performed on a silica surface, the lowest retraction velocity was 18 nm s^{-1} and the interaction time 10 s.

The cantilevers (Model MLCT-AUHW, Park Scientific Instruments, Sunnyvale, CA) used for the different experiments came from the same wafer. Calibration of the spring constant of each individual cantilever was performed by the thermal fluctuation technique (Florin et al., 1995). The stiffness obtained, i.e., 30 ± 5 mN m^{-1}, is consistent with the value given by the manufacturer (30 mN m^{-1}).

Sample preparation

Human fibrinogen was purchased from Sigma (F-4883, St. Louis, MO) and used without further purification. The protein was suspended in 10 mM phosphate-buffered saline buffer (pH 7.4 at 25°C), at a concentration of 20 mg/100 mL.

The fibrinogen was first adsorbed on the Si_3N_4 crystal, forming the AFM tip, by incubation of the cantilevers for 2 h in the protein solution. As the typical dimensions of a fibrinogen molecule are $5 \times 9 \times 45$ nm^3 (Lo et al., 1999) and as the tip apex ends with a roof-like shape not longer than 50 nm, only a small number of fibrinogen molecules are expected to be in a position to interact with the surface. The coated tip was then brought into contact with a hydrophilic silica surface (glass cover slip, Marienfeld, Germany), respectively, a freshly cleaved muscovite mica surface, in pure buffer. Before use, the surfaces were brought in contact with pure buffer during several hours for equilibration.

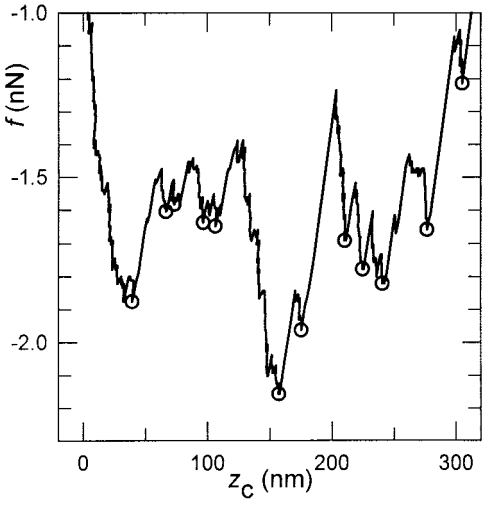

FIGURE 1 Part of a "force (f) vs. tip-to-surface distance (z_C)" curve corresponding to the detachment of fibrinogen from a silica surface. The superimposed circles label the significant minima that are assumed to represent rupture points.

Experimental results

From the measurement of the deflection of the cantilever as a function of the piezoelectric device position, one deduces the "force vs. tip-to-surface distance" curve (for details, see Gergely et al., 2001). For each retraction velocity considered, several consecutive approach/retraction cycles were performed. The "force vs. distance" curves are processed using the method described elsewhere (Gergely et al., 2001), which helps to identify the pertinent points on the curves (circles in Fig. 1), from which the rupture forces are deduced. Briefly, the algorithm that serves to process the experimental data detects the minima and maxima on a "force vs. distance" curve and evaluates the difference between a minimum and its neighboring maxima. On the other hand, the noise fluctuation, estimated by its standard deviation, is determined on the recording of the cantilever position in principle when the silica or mica surface is at rest (this part of the curve is not visible in Fig. 1). However, at a relatively high retraction velocity, the effect of hydrodynamic interaction between the cantilever and the surrounding liquid may appear (Fig. 2). One observes the presence of two plateaus: the second (final) plateau corresponds to the surface at rest, whereas the first plateau is due to a constant hydrodynamic force acting on the cantilever. This first plateau is obtained once the molecule is fully detached but the surface is still moving as shown by the upper curve representing the position of the piezoelectric crystal bearing the adhesion surface. In this case the first plateau is taken as the baseline for the evaluation of the rupture forces. A given minimum is recognized as a significant rupture point if the difference between this minimum and its

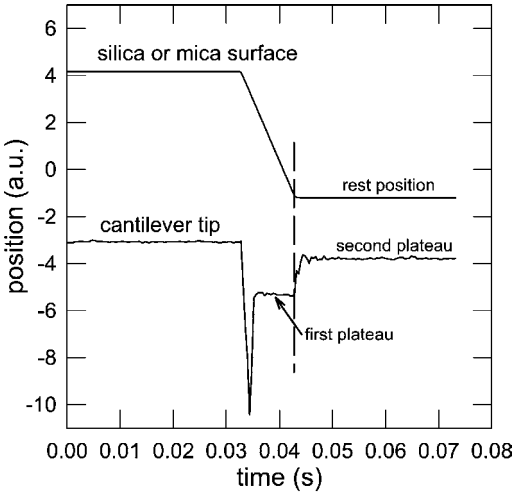

FIGURE 2 Time variation of the positions of the silica or mica surface and of the cantilever tip. During the retraction phase (segment with negative slope in the upper curve) one observes the rupture followed by a first plateau in the cantilever position. Once the surface comes to rest (lower horizontal segment in the upper curve), the cantilever moves to a second plateau. The jump from the first plateau to the second one reveals the hydrodynamic drag force. The dashed line shows the correspondence between the end of the first plateau and the end of the retraction phase.

two neighboring maxima is greater than the noise standard deviation multiplied by a factor to be chosen by the experimentalist on the basis of a preliminary calibration procedure (for further details, see Gergely et al., 2001). Because the number of cycles per retraction velocity is limited, we grouped all forces occurring within distance intervals of width 100 nm to reduce the statistical fluctuations on the mean force per interval (Gergely et al., 2000). At this point, we wish also to stress that we determine mean, not most probable rupture forces.

From the retraction velocity v_r one derives in principle the loading rate. As will be shown in the next section, the product $k_C v_r$ of the cantilever stiffness and the retraction velocity represents the apparent loading rate $\tilde{R}_f$, which coincides with the true loading rate R_f only if the molecule is much stiffer than the cantilever. In the present case, because the stiffness of the fibrinogen molecule is unknown it is not possible to estimate R_f. For this reason, the experimental results will be shown as a function of the retraction velocity that is an experimental parameter independent from any stiffness constant (neither that of the cantilever, nor that of the molecule).

The forces determined as outlined above for a silica surface and a mica surface are displayed in Fig. 3 *A* and *B*, respectively. The different points connected by a line correspond to a set of rupture forces measured with the same cantilever on which fibrinogen molecules have been adsorbed. Each point represents the average of 10 to 20 (in the case of the silica surface) and 40 to 50 (in the case of the mica surface) individual rupture forces. The uncertainty on these averages, as estimated by ± 2 times the standard error, lies in the range 70 to 240 pN for silica and 40 to 200 pN for mica. However, it is more interesting to notice that the dispersion corresponding to the silica results is appreciably larger than that corresponding to the mica surface. This may be due to the fact that the mica surface is much more homogeneous than the silica surface. It is thus expected that fibrinogen molecules can interact with the silica surface in much more different ways than with the mica surface, leading to a broader distribution of the measured forces under given experimental conditions. In addition, part of the silica results discloses a slight curvature in the high velocity domain, whereas the mica results appear as practically linear (provided that a logarithmic scale is used on both axes).

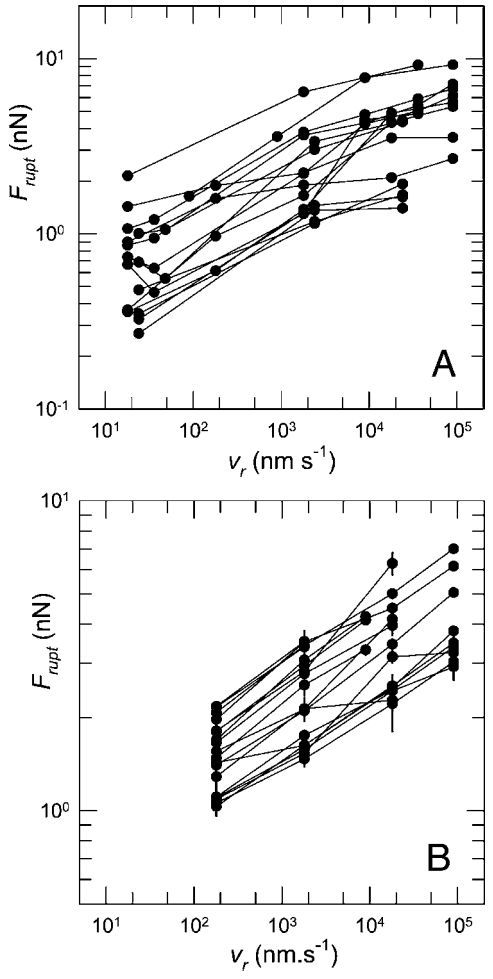

FIGURE 3 Experimental values of the mean detachment force of fibrinogen as a function of the retraction velocity: (*A*) silica surface, (*B*) mica surface.

MODELING

General features of the multi-bead-and-spring model

The detachment of a protein or a cell is modeled by an ensemble of n parallel springs submitted to an external pulling (or traction) force. These springs are related by a virtual rigid bar, B, kept parallel to the surface. The ith spring could be ascribed the stiffness k_i. We assume here, however, that all springs have the same stiffness k to simplify the model. An extra spring, of stiffness k_C and rest length ℓ_0, is attached to the bar opposite to the former n springs. The free end, C, of this spring is moved with the constant velocity v_C (which is the equivalent of v_r in the experiments). Thus, depending upon the value of k compared with that of k_C, the model corresponds to a stiff or a soft transducer in Seifert's terminology (Seifert, 2000) (see below). This distinction has also been made by Izrailev et al. (1997). All the springs are parallel to the z-direction, i.e.,

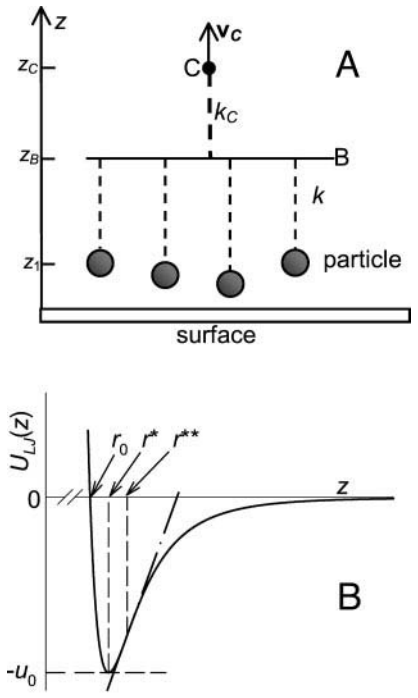

FIGURE 4 (*A*) Schematic representation of the multi-bead-and-spring model. The dashed lines represent springs: above the bar *B*, the cantilever of stiffness k_C, below the bar *B*, the "molecular" springs of stiffness *k*. All springs have the same rest length ℓ_0. Point *C* is moved with constant velocity v_C. The particles located at the lower end of the springs are assumed to interact with the surface through a Lennard-Jones potential represented in *B*. The slope of the dashed-dotted line represents the maximum of the gradient of the potential energy.

perpendicular to the surface, and, for the sake of simplicity, have the same rest length ℓ_0 (Fig. 4 *A*). Note that the value of ℓ_0 is arbitrary and has no incidence on the results because all "molecular" springs are identical.

At mechanical equilibrium of the system, the resulting force on *B* is zero. Now, suppose that point *C* be moved by a distance Δz_C during the time interval Δt, the free end of each of the *n* springs being immobile. To recover a null force on *B*, this latter moves over a distance Δz_B related to Δz_C by:

$$\Delta z_B = \frac{k_C}{K + k_C}\,\Delta z_C \tag{1}$$

in which $K = nk$. The increase of force applied to the *n* springs is therefore:

$$\Delta F = K\Delta z_B = \frac{Kk_C}{K + k_C}\,\Delta z_C \tag{2}$$

because within our model each spring is stretched by the same length Δz_B. The corresponding loading rate is then:

$$R_f = \frac{\Delta F}{\Delta t} = \frac{Kk_C}{K + k_C}\frac{\Delta z_C}{\Delta t} = \frac{Kk_C v_C}{K + k_C} \tag{3}$$

as the constant velocity of point *C* equals $\Delta z_C/\Delta t$ whatever the value of Δt. This makes clear that the apparent loading rate $\tilde{R}_f = k_C v_C$ is in general not the loading rate actually applied to the molecule to be detached from the surface. The actual loading rate R_f is smaller than $\tilde{R}_f$ or at most equal to it because the equivalent stiffness k_{eq} of the *n*-spring system, defined by $k_{eq} = Kk_C/(K + k_C)$, is smaller than or at most equal to k_C. If the global stiffness *K* is much smaller than the cantilever stiffness k_C (stiff transducer), Eq. 3 leads to:

$$R_f \approx nkv_C \ll \tilde{R}_f \tag{4}$$

On the other hand, if *K* is much larger than k_C (soft transducer), then:

$$R_f \approx k_C v_C = \tilde{R}_f \tag{5}$$

As will be seen below, the interpretation of our experimental force measurements by means of the multi-bead-and-spring model suggests that fibrinogen behaves as an assembly of parallel springs, each being soft if compared with the cantilever.

It follows from Eq. 3 that the loading rate on a bond is, in general, not uniquely determined by the pulling velocity v_C and the stiffness k_C of the pulling spring, i.e., of the cantilever. In addition, it follows from Eqs. 4 and 5 that the loading rate per bond, $r_f = R_f/n$, is independent from the number of bonds in the limit of a very stiff transducer, whereas it is inversely proportional to the number of bonds in the limit of a very soft transducer. Indeed, Eqs. 1 to 5 give idealized definitions of both z_B and R_f because the particles are in fact not immobile. We shall return to this point below.

To model the interaction of a molecule or a cell with a surface, we assume that it can be represented by the ensemble of *n* parallel springs discussed above and a particle fixed at the free end of each of these springs. Each particle experiences a potential energy due to the surface. We assume that at a given distance from the surface this energy is identical for all particles and we represent it by a Lennard-Jones (LJ) 12-6 well:

$$U_{LJ}(z_i) = 4u_0\left[\left(\frac{r_0}{z_i}\right)^{12} - \left(\frac{r_0}{z_i}\right)^{6}\right] \tag{6}$$

in which z_i is the distance of the *i*th particle to the surface. This LJ potential energy is determined by two parameters, the depth $-u_0$ and the range r_0, both assumed to be the same for all particles (Fig. 4 *B*). Moreover, one can define the two characteristic parameters r^* and r^{**} that correspond to the distances where the LJ force F_{LJ} is zero, i.e., where the LJ potential energy is minimum, and the most attractive, respectively. These distances are the positive, real roots of the equations

$$\left.\frac{dU_{LJ}}{dz_i}\right|_{z_i=r^*} = 0 \quad \text{and} \quad \left.\frac{d^2U_{LJ}}{dz_i^2}\right|_{z_i=r^{**}} = 0,$$

and are given by

$$r^* = 2^{1/6} r_0 \quad \text{and} \quad r^{**} = \left(\frac{26}{7}\right)^{1/6} r_0.$$

Note that

$$|F_{LJ}(r^{**})| = (\nabla U_{LJ})_{z=r^{**}} = \max(\nabla U_{LJ}) = \frac{504}{169}\frac{u_0}{r^{**}}$$

is the maximum resistance the LJ well can oppose to the detachment of a particle.

Initially, each particle is located at $z_i = r^*$, i.e., at the deepest point of its potential well. The movement of a particle is ruled by the Langevin equation at one dimension because in the present model the particles are constrained to move exclusively along the z-direction perpendicular to the surface. For the ith particle ($1 \le i \le n$), this equation gives the displacement Δz_i corresponding to the time interval Δt (Ermak and McCammon, 1978):

$$\Delta z_i = \frac{DF_i}{k_B T}\Delta t + (\Delta z_{random})_i \tag{7}$$

in which F_i is the signed modulus of $\mathbf{F}_i$, which is the vector sum of the spring force, $\mathbf{f}_i$, exerted by the ith spring on the ith particle and of the interaction force $(\mathbf{F}_{LJ})_i$ between the ith particle and the surface. The spring force modulus is given by Hooke's law: $f_i = k(z_B - z_i - \ell_0)$. Furthermore, D represents the diffusivity of a particle, assumed to be the same for all particles and independent of its location, k_B is the Boltzmann constant, and T the absolute temperature. The diffusivity is related to the damping factor ξ by $D = k_B T/\xi$. Finally, $(\Delta z_{random})_i$ represents the random, Brownian displacement that is a normal variable of mean equal to zero and variance equal to $2D\Delta t$. The duration Δt of a step is determined so that the particle that experiences the largest resulting force, $F_{max} = \max(|F_i|)$, does not move, on the average, over more than the small distance εd in which $\varepsilon \ll 1$ and $d = r^{**} - r^*$. Thus, the magnitude Δt of a time step is determined by the positive root of the equation (derived from Eq. 7):

$$\left(\frac{DF_{max}}{k_B T}\right)^2 (\Delta t)^2 + 2D\Delta t = (\varepsilon d)^2 \tag{8}$$

Note that Δt is recomputed for each step because F_{max} varies from step to step.

During its movement, each particle explores an energy landscape resulting from the addition of the LJ potential energy and the mechanical potential energy due to its spring. The total potential energy $U(z)$ for a particle is therefore given by:

$$U(z) = 4u_0\left[\left(\frac{r_0}{z}\right)^{12} - \left(\frac{r_0}{z}\right)^{6}\right] + \frac{1}{2}k(z_B - z - \ell_0)^2 \tag{9}$$

in which z is any positive distance from the surface. The actual position z_i of a particle is one particular value of z. Apart from the two infinite maxima always located at $z = 0$ and $z = \infty$, the function $U(z)$ displays either one finite minimum, or two finite minima and one finite maximum following the value of z_B and the values of u_0, r_0, and k. The existence of a finite maximum, located at $z = z_{ts}$, where the subscript *ts* stands for "transition state," reflects the existence of a finite energy barrier that must be crossed by the particle to escape from the LJ well. It must be pointed out that for the transition state to be defined, it is necessary, although not sufficient, that $d^2U/dz^2 < 0$ over a nonvanishing interval $[z_1, z_2]$. This requires that the polynomial $26 - 7\zeta^6 + (kr_0^2/24u_0)\zeta 14$ possesses two real positive roots, which happens if kr_0^2/u_0 is smaller than $72(2/13)^{4/3} \approx 5.935$. If this condition is not fulfilled, the detachment process results no longer from a thermal diffusion over an energy barrier and fits therefore not in the scope of the present study. Thus, in the following, we examine exclusively cases where the triplets (u_0, r_0, k) permit the existence of z_{ts}.

Note that because z_B depends on the fluctuating position of the particles (Eq. 10 below), it is itself fluctuating and so is z_{ts}. Nevertheless, because we assume that all bonds are identical, the barrier position z_{ts}, when it is defined, is the same for all particles at a given time. As long as z_B is smaller than a given value, no finite barrier exists and the detachment is impossible. Once z_B exceeds the value $(\nabla U_{LJ})_{z=r^{**}}/k + r^{**} + \ell_0$, the barrier disappears; the escape is then achieved whatever the location of the particles. Between these two bounds, the finite barrier exists. Then, a particle may be detached if its position satisfies the necessary condition $z_i > z_{ts}$.

At the beginning of the simulation of a detachment cycle, the bar B is placed at the distance z_B from the surface so that the sum of the spring tensions be zero, i.e., $z_B = r^* + \ell_0$. The position z_C is fixed to $z_B + \ell_0 = r^* + 2\ell_0$ so that the tension on the pulling spring be zero too. The time t is then set to zero for the start of the detachment process. From there on, the algorithm proceeds in the following way. 1) The spring force and the LJ force for each particle are determined. 2) The time step Δt is evaluated using Eq. 8. 3) The n particles are moved as prescribed by Eq. 7. 4) The position of point C is updated by adding $\Delta z_C = v_C \Delta t$ to its former position to obtain its new position z_C. 5) The position of B is recomputed so that the total force on it be again zero:

$$z_B = \frac{k\sum_{i=1}^{n}(z_i + \ell_0) + k_C(z_C - \ell_0)}{nk + k_C}$$

$$= \frac{k\sum_{i=1}^{n}(z_i - r^*) + k_C v_C t}{nk + k_C} + r^* + \ell_0 \tag{10}$$

Note that this definition of z_B takes into account the actual positions of the particles that are in general not equal to r^*.

For this reason Eq. 10 is not rigorously equivalent with Eq. 1 based on the assumption that the particles were immobile. Eq. 10 renders clear why z_B is a fluctuating variable, whereas z_C is purely deterministic. 6) With this updated value of z_B, the system is ready for the next step, i.e., the algorithm may return to (1) Prior to this, however, one has to check whether the particles have crossed their energy barrier. If at least one particle is located on the left of the top of the barrier ($z_i < z_{ts}$), or if no finite barrier exists although $z_B < (\nabla U_{LJ})_{z=r^{**}}/k + r^{**} + \ell_0$, the value of the tension $F_C = k_C(z_C - z_B - \ell_0)$ of the pulling spring, equal to the sum of the tensions of the n springs, is taken as the current rupture force F_{rupt}. In principle, the detachment is achieved if all particles have crossed the energy barrier if it exists or if the barrier has disappeared. However, to reduce strongly the probability of recrossing the barrier (or, in other words, of rebinding to the surface), each particle, once detached, must in addition reach a position where its potential energy is lower than its potential energy at $z = z_{ts}$ by 5 k_BT (this is an arbitrary choice) if the barrier exists, or lower than the potential energy it would have at $z = r^{**}$ by 5 k_BT too, if the barrier has been eliminated. As long as the molecule is not considered as detached, the algorithm proceeds to (1). If, in contrast, the molecule is detached according to the aforementioned rules, the cycle terminates.

This procedure is continued until a preset number of cycles are completed to build up a sample of rupture forces corresponding to the same simulation parameters, except that the random contributions to the displacement of the particles are different for each cycle.

The multi-bead-and-spring model (with different values of n) will be used to interpret the experimental data relative to the detachment of fibrinogen from silica and mica surfaces. These examples are used to illustrate the general features of the model. However, prior to this, we shall examine the properties of the model, especially in its simplest version, i.e., when $n = 1$. This will allow us to get a better understanding of most of the parameters entering the model. We shall then proceed to the model with $n > 1$.

Properties of the 1-bead-and-spring model

The model described above has been used to predict the rupture force F_{rupt} as a function of the retraction (or pulling) velocity v_C, for various combinations of the parameters k, D, u_0, and r_0, in the particular case of $n = 1$. For each combination of the parameters investigated, a number of cycles (most often $n_{cycles} = 10$) were repeated for a given value of v_C. From them, one deduces the mean rupture force and the uncertainty taken as two times the standard error (SE) on the mean. Throughout the simulations, the stiffness k_C of the cantilever and the temperature T were kept fixed to values similar to their experimental values, i.e., 0.03 N m^{-1} and 300 K, respectively, and the parameter ε was fixed to 0.01.

It is difficult to assign *a priori* a value to D. Its approximate order of magnitude was determined on the basis of data given by Evans (1999). For a damping factor of 2×10^{-11} N s^{-1} m^{-1} this author indicates an off-rate on the order of 2×10^9 to 2×10^{10} s^{-1}. We had found for the detachment of fibrinogen from a silica surface (Gergely et al., 2000) an off-rate of 0.2 to 0.4 s^{-1}. Assuming that the off-rate is inversely proportional to the damping factor, and that the parameters related to the potential energy well can be disregarded, leads to an estimate of the diffusivity on the order of 0.2 to 4×10^{-20} m^2 s^{-1}. A few preliminary simulations indicated that for the experiments we have at hand D should lie in the region 10^{-20} to 10^{-18} m^2 s^{-1}. Thus, in the first series of simulations aimed at obtaining the "F_{rupt} vs. v_C" relation, we used $u_0 = 5\ k_BT$, $r_0 = 0.1$ nm and four combinations of D (in m^2 s^{-1}) and k (in N m^{-1}), namely (10^{-18}, 0.0003), (10^{-20}, 0.0003), (10^{-18}, 3), and (10^{-20}, 3).

The four series of rupture forces are represented in Fig. 5 *A*, in which it is seen that they do not coincide. Nonetheless, the four series display quite similar shapes. It may, therefore, be interesting to redraw these results using a conveniently scaled abscissa variable. A quite natural choice is to use R_f (not $\tilde{R}_f$) instead of v_C. This is, however, not sufficient because a relative change in D can be compensated for by the same relative change of v_C. Hence, it appears that R_f/D is a better choice. Because this is not a dimensionless variable, we use the reduced retraction rate ρ, proportional to R_f/D, defined by:

$$\rho = \frac{R_f r_0^3}{D k_B T} = \frac{nk k_C v_C r_0^3}{(nk + k_C) D k_B T} \tag{11}$$

as the abscissa variable. This general expression for ρ, i.e., valid for any n, found here empirically, has a rational basis as shown in the Appendix. Note that the force can also be made dimensionless if one defines the reduced force by, e.g., $\phi = F_{rupt}/n|F_{LJ}(r^{**})|$. It appears in Fig. 5 *B* that at fixed k, the data corresponding to different diffusivities do strictly match. With respect to the parameter D the scaling works thus perfectly over the entire range of loading rates investigated (seven orders of magnitude). At fixed D, the data corresponding to $k = 0.0003$ and 3 N m^{-1} agree fairly well as long as $\rho \geq 1$, whereas they diverge gradually as ρ decreases from 1 to 10^{-2}. The breakdown of the scaling law at small values of ρ reveals the increasing importance of the random component of the displacement of the particle as discussed in the Appendix, which is enhanced by the stiffness k of the "molecular" spring.

Since the variable ρ contains r_0 (as r_0^3), it was also interesting to perform simulations with another value of r_0, for instance $r_0 = 0.02$ nm instead of 0.1 nm, whereas keeping $D = 10^{-18}$ m^2 s^{-1}, $k = 0.0003$ or 3 N m^{-1}, and $u_0 = 5\ k_BT$. The corresponding rupture forces are shown in Fig. 6 *A* as a function of the pulling velocity. Clearly, the plateau height increases as r_0 decreases (compare with the results corresponding to $r_0 = 0.1$ nm reproduced in Fig. 6

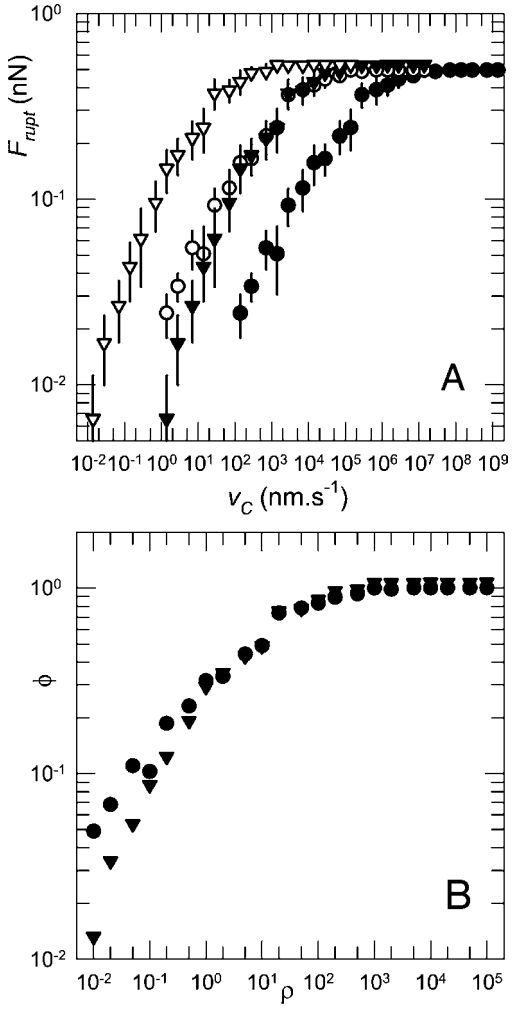

FIGURE 5 (*A*) Rupture force predicted by the 1-bead-and-spring model as a function of the pulling velocity. The four sets of data correspond to the same potential energy depth $-u_0 = -5\ k_BT$ at $T = 300$ K, and range $r_0 = 0.1$ nm, and the same cantilever stiffness $k_C = 0.03$ N m^{-1}. They differ by the value of the "molecular" spring stiffness k or the diffusivity D: $k = 0.0003$ N m^{-1} and $D = 10^{-18}$ m^2 s^{-1} (*closed disks*), $k = 0.0003$ N m^{-1}, and $D = 10^{-20}$ m^2 s^{-1} (*open disks*), $k = 3$ N m^{-1} and $D = 10^{-18}$ m^2 s^{-1} (*closed triangles*), $k = 3$ N m^{-1} and $D = 10^{-20}$ m^2 s^{-1} (*open triangles*). Each data point represents the average over 10 cycles and the error bars represent twice the standard error on the mean. (*B*) Same data transformed to reduced force as a function of reduced loading rate. Open symbols are masked by the corresponding closed symbols.

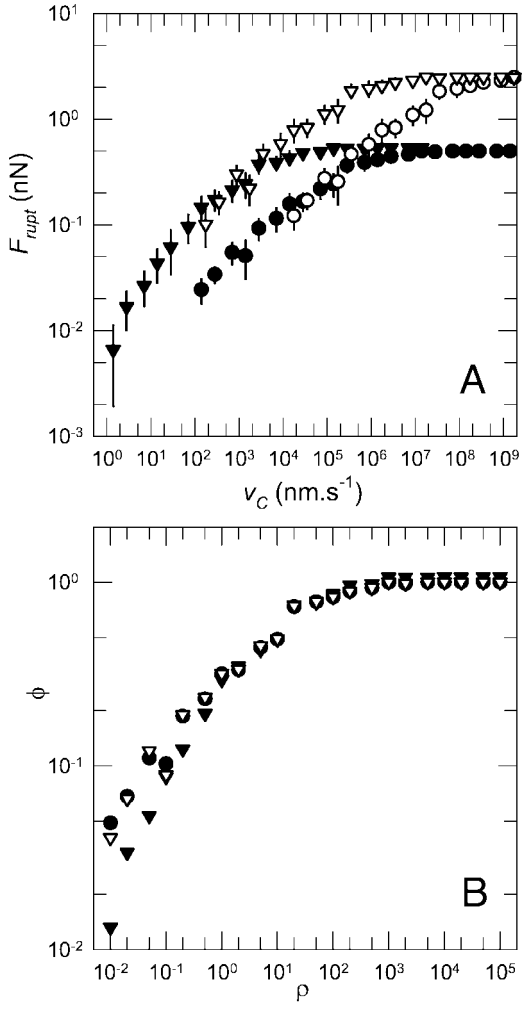

FIGURE 6 (*A*) Rupture force predicted by the 1-bead-and-spring model as a function of the pulling velocity. The four sets of data correspond to the same potential energy depth $-u_0 = -5\ k_BT$ at $T = 300$ K, the same diffusivity $D = 10^{-18}$ m^2 s^{-1} and the same cantilever stiffness $k_C = 0.03$ N m^{-1}. They differ either by the potential energy range r_0 or the value of the "molecular" spring stiffness k: $r_0 = 0.1$ nm and $k = 0.0003$ N m^{-1} (*closed disks*) or $k = 3$ N m^{-1} (*closed triangles*), $r_0 = 0.02$ nm and $k = 0.0003$ N m^{-1} (*open disks*) or $k = 3$ N m^{-1} (*open triangles*). Each data point represents the average over 10 cycles, and the error bars represent twice the standard error on the mean. (*B*) Same data transformed to reduced force as a function of reduced loading rate. Note that the open and closed disks coincide.

A). Fig. 6 *B* demonstrates that the plateau is to a high degree of accuracy proportional to the maximum resistance of the potential well, which varies as the reciprocal of the range of the well. Moreover, it appears that the reduced forces ϕ corresponding to $k = 0.0003$ and 3 N m^{-1}, when $r_0 = 0.02$ nm, agree quasi perfectly, whereas those corresponding to $k = 0.0003$ and 3 N m^{-1}, when $r_0 = 0.1$ nm, diverge (see also Fig. 5 *B*) when $\rho < 1$. It follows from this observation that not only the maximum gradient of the potential energy is important but that there is an interplay between this maximum gradient and the stiffness of the spring.

Finally, as regards the system with $n = 1$, we have determined the rupture force as a function of the pulling velocity for various values of the well depth ($u_0 = 2.5$, 5, 10, 20, and 40 k_BT), at fixed values of r_0 (0.1 nm), k (3 N m^{-1}), and D (10^{-18} m^2 s^{-1}). Fig. 7 *A* shows that changing u_0 affects the value of F_{rupt} at a given pulling velocity, as expected. One also finds that representing the simulation results using the scaled abscissa and ordinate variables leads not to a unique curve (Fig. 7 *B*), except in the high velocity domain. This shows again that, when the maximum gradient of the potential energy well changes, the relative importance

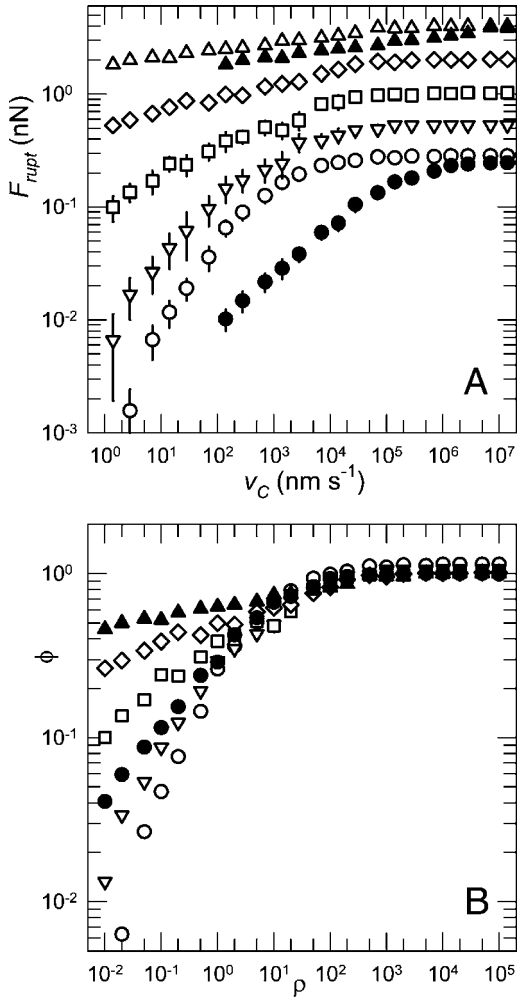

FIGURE 7 (*A*) Rupture force predicted by the 1-bead-and-spring model as a function of the pulling velocity. The seven sets of data correspond to the same potential energy range $r_0 = 0.1$ nm, the same diffusivity $D = 10^{-18}$ m^2 s^{-1} and the same cantilever stiffness $k_C = 0.03$ N m^{-1}. They differ by the value of either the potential energy depth $-u_0$ (at $T = 300$ K) or the "molecular" spring stiffness k: $u_0 = 2.5\ k_BT$ and $k = 3$ N m^{-1} (*open disks*), $u_0 = 5\ k_BT$ and $k = 3$ N m^{-1} (*open triangles down*), $u_0 = 10\ k_BT$, and $k = 3$ N m^{-1} (*open squares*), $u_0 = 20\ k_BT$ and $k = 3$ N m^{-1} (*open diamonds*), $u_0 = 40\ k_BT$ and $k = 3$ N m^{-1} (*open triangles up*), $u_0 = 2.5\ k_BT$ and $k = 0.0003$ N m^{-1} (*closed disks*), $u_0 = 40\ k_BT$ and $k = 0.0003$ N m^{-1} (*closed triangles up*). Each data point represents the average over 10 cycles (except for $u_0 = 2.5\ k_BT$ where 40 cycles were performed) and the error bars represent twice the standard error on the mean. (*B*) Same data transformed to reduced force as a function of reduced loading rate. Open and closed symbols are indistinguishable for $u_0 = 40\ k_BT$.

of the thermal fluctuations changes and influences significantly the measured rupture force. The lower the maximal resistance of the well, the more sensitive the rupture force to the pulling velocity. However, here also, it is interesting to discuss the results when k is considerably smaller. Therefore, we have added force curves corresponding to a soft spring ($k = 0.0003$ N m^{-1}). As can be seen in Fig. 7 *A*, the soft-spring curves corresponding to $u_0 = 2.5$ and $40\ k_BT$ differ from their respective hard-spring counterparts, merely because the same velocity does not produce the same loading rate when the stiffness is changed as was already seen in Fig. 5. Moreover, as can be seen in Fig. 7 *B*, the scaled force curves corresponding to $k = 3$ and 0.0003 N m^{-1}, when $u_0 = 2.5\ k_BT$, do not coincide over the whole ρ-domain investigated. This confirms the finding of Fig. 5 *B* that the maximum gradient of the well may not be sufficient to characterize the force curve. However, if u_0 is increased, the sensitivity to k tends to disappear as demonstrated by the excellent coincidence of the scaled force curves corresponding to $k = 3$ and 0.0003 N m^{-1} when $u_0 = 40\ k_BT$.

In Fig. 8 *A* and *B*, we give two illustrative examples of the evolution of the position of the particle (trajectories in the (z_C, z)-plane) and of the traction force F_C felt by the particle that is identical with the cantilever force because there is only one bond, as a function of the position of point *C*. In the two cases examined, $u_0 = 5\ k_BT$, $r_0 = 0.1$ nm, $k = 3$ N m^{-1}, and $D = 10^{-18}$ m^2 s^{-1}. When the pulling velocity is fast (Fig. 8 *A*, $\rho = 10^2$, $v_C \approx 14{,}000$ nm s^{-1}), which corresponds to the plateau region in Fig. 5 *A*, the particle does not move over a large distance (a few hundredths of nm), whereas point *C* moves over ≈17 nm. Then, the traction force approaches the maximum resistance of the well (≈0.5 nN, see insert). Thus, the detachment of the molecule is mainly due to the rapid increase of the force, which eliminates the energy barrier rather than to the movement of the molecule (even at the end of the cycle the distance traveled by the particle is hardly equal to 0.1 nm, i.e., less than r_0). The thermal fluctuations play here a minor role as could already be deduced from the fact that $F_{rupt} \approx \max(\nabla U_{LJ})$ (see Fig. 5 *A*). This is further confirmed by comparing the force F_C obtained with fluctuations to its counterpart when fluctuations are inhibited, as represented in the insert of Fig. 8 *A*. It appears that both forces are indistinguishable. The same simulation at a slow pulling velocity (Fig. 8 *B*, $\rho = 10^{-1}$, $v_C \approx 14$ nm s^{-1}) shows a totally different picture. Now, there is first an induction period during which the particle fluctuates in the well without any trend. Once $z_C - 2\ell_0$ attains 0.8 to 0.9 nm, the pulling force is still far from the maximum resistance of the well equal to ≈0.5 nN (see insert). Nonetheless, the molecule position begins to grow very rapidly. Because the velocity is small, the time needed to reach the maximum force is by far too long so that fluctuations could develop long before and produce the rupture. Then, the particle overcomes the maximum resistance of the well even though it is submitted to a traction force that is much smaller than this maximum resistance. Once the particle is far enough from the surface (i.e., on the right hand side of the barrier, which still exists), the pulling force, although weak, is sufficient to pull it definitively away. This mechanism leads to the moderate rupture force observed at this low velocity, as already mentioned by others (Evans and Ritchie, 1999). It may be noticed

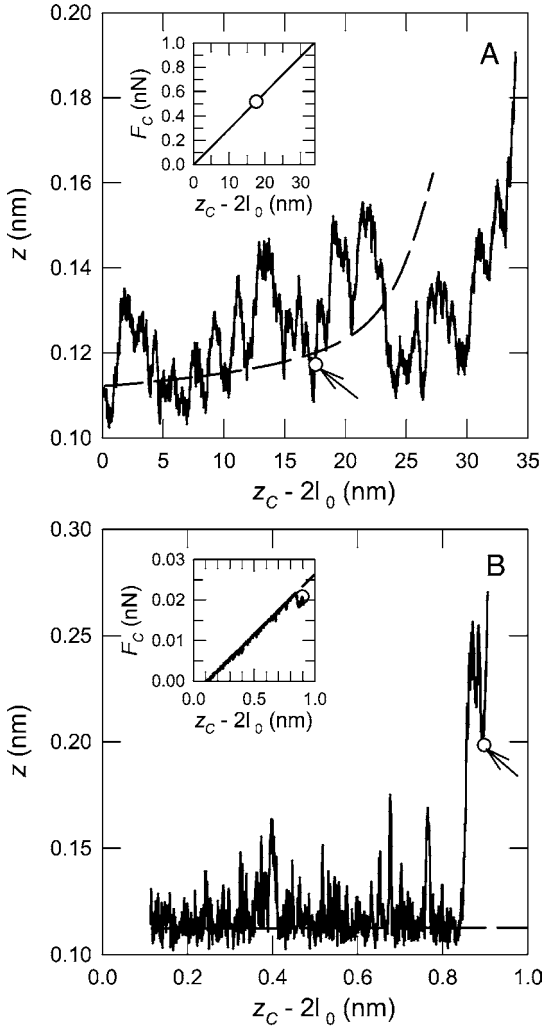

FIGURE 8 Examples of trajectories in the (z_C, z)-space. The inserts give the force felt by the cantilever spring as a function of its position z_C. The dashed lines indicate the results that would be obtained in the absence of thermal fluctuations (deterministic detachment process). The parameters common to the two parts of the figure are: $u_0 = 5\ k_BT$ at $T = 300\ K$, $D = 10^{-18}$ m^2 s^{-1}, $k = 3$ N m^{-1}. The other simulation parameters are as follows: (*A*) $r_0 = 0.1$ nm and $\rho = 10^2$ (correspond to $v_C = 13{,}944$ nm s^{-1}), (*B*) $r_0 = 0.1$ nm and $\rho = 10^{-1}$ (correspond to $v_C = 13.944$ nm s^{-1}). In *a* and *b*, the detachment point is marked by a white dot. In *a*, the detachment occurs after elimination of the barrier, whereas in *b* the thermal fluctuation causes the detachment long before the elimination of the barrier. As a result, the force is much smaller in *B* than in *A*.

that until the detachment occurs, the force is not greatly different from the force that would act on the particle if the process was deterministic (see insert). However, once the thermal fluctuations of the position of the particle have caused the jump over the barrier, the actual trajectory differs from the deterministic one.

The detachment process can thus be seen as a diffusion process in an energy landscape, as suggested by Evans, where the energy depends on both the distance to the surface, z, and the time, t. The particle diffuses in the z direction, whereas it moves uniformly along the t axis. At each time t, a particle is located in a potential well $U_B(z, t) = U_{LJ}(z) + \frac{1}{2}k(z_B - z - \ell_0)^2$ when the bar B is taken as the reference. However, z_B is a random variable because it depends on z (see Eq. 10). The position of B can therefore not be expressed as a simple function of time. Thus, for the purpose of graphical representation, it is easier to take point C as the reference and write $U_C(z, t) = U_{LJ}(z) + \frac{1}{2}k_{eq}(z_C - z - 2\ell_0)^2$. Upon replacing z_C by $v_Ct + r^* + 2\ell_0$, one gets $U_C(z, t) = U_{LJ}(z) + \frac{1}{2}k_{eq}(v_Ct + r^* - z)^2$. Notice that the rest length ℓ_0 no longer appears in this expression, confirming that it is not a physically relevant parameter. In addition, we subtract from $U_C(z, t)$ the potential energy that would be stored in the springs if the particle did to move, i.e., $U_C(r^*, t)$. In this way, we represent the trajectory of the particle on the energy surface defined by $\Delta U(z, t) = U_C(z, t) - U_C(r^*, t)$. The detachment process occurs either when the barrier disappears or when the particle, while moving in the direction of increasing z, crosses the last time the ridge on the energy landscape. Examples of trajectories in the (t, z, ΔU)-space are shown in Fig. 9 *A* and *B*. Fig. 9 *A* corresponds to a fast retraction velocity, namely $v_C = 10{,}000$ nm s^{-1}. In such a case, as already evoked, the thermal fluctuations do generally not contribute significantly to the detachment. Indeed, a few attempts to cross the ridge are observed, but they do not lead to the detachment. This latter occurs later on, once the barrier is eliminated. This means that the external force had to reach a value on the order of the maximum resistance of the well. In Fig. 9 *B* the retraction velocity is lowered to 100 nm s^{-1}. One can observe several escapes over the barrier followed by a recrossing, i.e., a diffusion back to the surface, until the particle diffuses definitively away from the surface, much earlier than the elimination of the barrier. In this case, the detachment is clearly due to the thermal fluctuations.

Comparison of the 1-bead-and-spring model predictions with fibrinogen detachment data

Let us now try to answer the question: is it possible to represent the experimental "rupture force vs. retraction velocity" curves, related to fibrinogen in contact with silica or mica surfaces, using the spring-and-bead model with only one spring and one particle that represent the molecule, provided that four parameters are free, namely the stiffness of the molecule, k, the diffusivity, D, as well as the depth $-u_0$ and the range r_0 of the interaction potential energy?

The experimental results for fibrinogen adsorbed on silica (Fig. 3 *A*) suggest that the plateau of the rupture force, as obtained using the model, should be located at a height on the order of 5 nN. Now, the level of the plateau is determined by the maximum of the gradient of the interaction energy U_{LJ}, which is itself proportional to the ratio u_0/r_0. To obtain a plateau value of ~5 nN, one needs $(u_0/k_BT)/r_0 \approx$

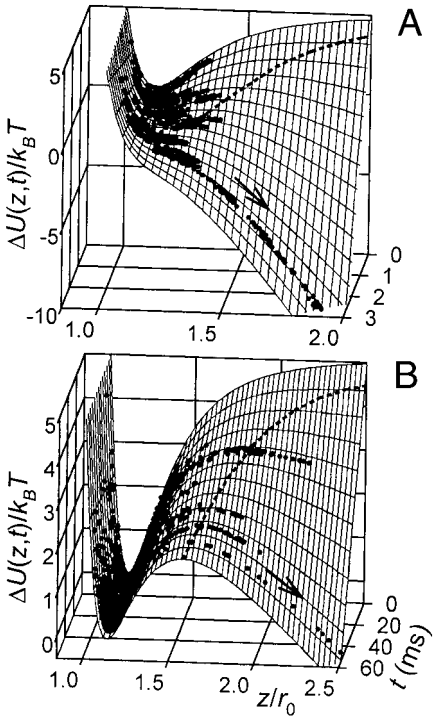

FIGURE 9 Illustrative examples of potential energy landscapes for a particle submitted to a Lennard-Jones potential due to the vicinity of a surface and a mechanical potential energy due to both its spring and the cantilever, as a function of time t and particle position z. The dashed line represents the ridge of the landscape. Detachment occurs either when the ridge disappears (A) or when the particle crosses definitively this ridge (B). The dots represent successive positions of the particle during the detachment process (note that only part of the points has been represented for the sake of clarity). The two examples correspond to a retraction velocity v_C equal to 10,000 nm s^{-1} (A) and 100 nm s^{-1} (B). The other parameters are $u_0 = 5\ k_BT$ at $T = 300$ K, $r_0 = 0.1$ nm, $D = 10^{-18}\ m^2\ s^{-1}$, $k_C = 0.03$ N m^{-1}, and $k = 3$ N m^{-1} in both cases.

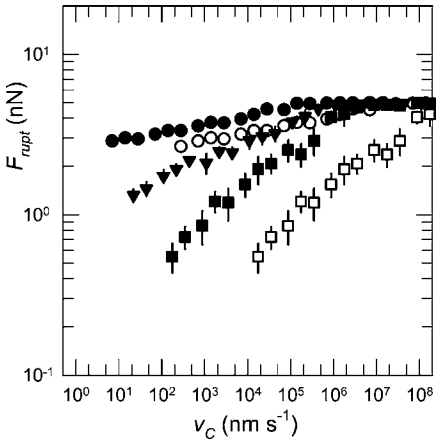

FIGURE 10 Rupture force predicted by the 1-bead-and-spring model as a function of the pulling velocity. The five sets of data correspond to the same ratio $(u_0/k_BT)/r_0 = 500\ nm^{-1}$ at $T = 300$ K, the same diffusivity $D = 10^{-18}\ m^2\ s^{-1}$ and the same cantilever stiffness $k_C = 0.03$ N m^{-1}. They differ by the potential energy depth $-u_0$ and range r_0, or the value of the "molecular" spring stiffness k: $u_0 = 50\ k_BT$, $r_0 = 0.1$ nm and $k = 3$ N m^{-1} (*closed disks*), $u_0 = 20\ k_BT$, $r_0 = 0.04$ nm and $k = 3$ N m^{-1} (*closed triangles*), $u_0 = 10\ k_BT$, $r_0 = 0.02$ nm and $k = 3$ N m^{-1} (*closed squares*), $u_0 = 50\ k_BT$, $r_0 = 0.1$ nm and $k = 0.0003$ N m^{-1} (*open disks*), $u_0 = 10\ k_BT$, $r_0 = 0.1$ nm and $k = 0.0003$ N m^{-1} (*open squares*). Each data point represents the average over 10 cycles, and the error bars represent twice the standard error on the mean.

500 nm^{-1}. If one chooses $r_0 = 0.1$ nm, it follows that u_0 must be equal to $\sim 50\ k_BT$. If one refers to Fig. 10 (closed disks), one sees immediately that for this combination of u_0 and r_0, the "force vs. velocity" curve is much too flat if compared with the experimental trend (Fig. 3 *A*). As we know (see Fig. 5), for the 1-bead-and-spring model the slope is to a large extend independent from the stiffness of the spring (compare open and closed disks in Fig. 10) as well as from the diffusivity, so that neither k nor D can help to adapt the slope of the simulated curve to that of the experimental one. Thus, to increase the slope, it is necessary to reduce the depth of the potential well (see Fig. 7). Nevertheless, because $(u_0/k_BT)/r_0 = 500\ nm^{-1}$ is required, r_0 must be reduced simultaneously in the same proportion as u_0. With $k = 3$ N m^{-1} and $D = 10^{-18}$ m^2 s^{-1}, we have simulated the rupture force F_{rupt} as a function of the retraction velocity for two other combinations of u_0 and r_0 (closed triangles and squares in Fig. 10). Comparing these results with those in Fig. 3 reveals that the slope of the linear part of the experimental curve is best reproduced by the simulation corresponding to $u_0 = 10\ k_BT$ and $r_0 = 0.02$ nm (closed squares). Note that with a soft spring the same slope is obtained (open squares in Fig. 10). However, the simulated force curve, with $k = 3$ N m^{-1}, is shifted by one to two orders of magnitude toward the high velocities if compared with the experimental data. To bring the simulated curve in better match with its experimental counterpart one can in principle change either k or D, or both. However, k being high compared with k_C, increasing it further would hardly change the factor $k/(k + k_C)$, so that it is impossible to shift significantly the simulated curve toward smaller velocities by increasing k in the present context. The sole possibility remains to decrease D (see Fig. 5). We have therefore simulated the rupture forces corresponding to $u_0 = 10\ k_BT$, $r_0 = 0.02$ nm, and $D = 10^{-18}$, 10^{-19}, and 10^{-20} m^2 s^{-1}, k being kept fixed to 3 N m^{-1}. In this way, we could verify that, as expected, the slope is unaltered by the change in D. It must be realized that an appropriate change in D, applied to the force curve corresponding to $k = 0.0003$ N m^{-1}, would also have led to the desired shift, hence to the agreement with the experimental data. It is then clear that k and D are practically undetermined in this approach. Comparing these simulations with the experimental data (Fig. 3) reveals that the value $D = 10^{-19}$ m^2 s^{-1} gives a satisfactory reproduction of the experimental data, when $k = 3$ N m^{-1}. It follows that the 1-bead-and-spring model is suited to the interpretation of detachment experiments of molecules from

surfaces, although with a limited capacity of ascribing numerical accurate values to part of the parameters entering the model. More precisely, the ratio u_0/r_0 is fixed by the maximum rupture force that should be attained at high retraction velocity, whereas k_{eq}, hence k, and D cannot be determined separately.

The reasonably good agreement could, however, only be obtained for a value of r_0 on the order of 0.02 nm. Such a small range for the potential energy well is physically unrealistic, showing that the 1-bead-and-spring model is not able to account correctly for the experimental results. For this reason, we have investigated the possibility to reproduce equally well the experimental data with a multi-bead-and-spring model with the requirement that a larger value for r_0 should be found.

Comparison of the multi-bead-and-spring model predictions with fibrinogen detachment data

The rupture force corresponding to the plateau in the high velocity region is proportional to the number n of springs. To preserve the plateau height at ≈5 nN, we thus write $n(u_0/k_BT)/r_0 = 500\ \text{nm}^{-1}$. There are mainly two possibilities to comply with this constraint: either r_0 is kept fixed and u_0 is varied with n, or u_0 is kept fixed and r_0 is varied with n. Obviously, the second option is here appropriate because increasing n leads to increase r_0, which is the goal indicated above. As a consequence we keep $u_0 = 10\ k_BT$ and use $r_0 =$ 0.04, 0.08, and 0.16 nm for $n = 2$, 4, and 8, respectively (Fig. 11 *A*). For the sake of completeness we have also drawn the curve corresponding to $n = 1$. In all these cases, the stiffness per spring was fixed to $k = 3\ \text{N m}^{-1}$. As can be seen, the slope decreases when n increases (see also the reduced variable representation in Fig. 11 *B*). This implies that reaching a reasonable value of r_0 with u_0 and k fixed to $10\ k_BT$ and $3\ \text{N m}^{-1}$, respectively, is not compatible with a slope in agreement with the experimental one.

Nevertheless, we have to reconsider the observation that k has practically no influence on the slope as follows from the analysis of the 1-bead-and-spring model (see above). We have therefore repeated the simulations corresponding to $n = 2$, 4, and 8, using soft springs to represent the molecule: $k = 0.0003\ \text{N m}^{-1}$ instead of $3\ \text{N m}^{-1}$ (Fig. 12 *A*). By comparing Figs. 11 *A* and 12 *A*, one can see that a change in k has a growing influence on the slope when n increases: for a given value of $n \geq 2$, a small value of k leads to a steeper slope than does a large value of k. In addition, a small value of k leads to a nearly unique curve when the reduced variables are used (Fig. 12 *B*). Once $k = 0.0003\ \text{N m}^{-1}$, with $k_C = 0.03\ \text{N m}^{-1}$, we have clearly a hard transducer ($k \ll k_C$ and even $nk \ll k_C$), so that it is not useful to reduce k further: no supplementary increase of the slope is expected. This statement has been verified by using $k = 0.00003\ \text{N m}^{-1}$ in the 8-bead-and-spring model.

In Fig. 13, the rupture forces predicted using 4 and 8 soft springs are compared with the experimental data corresponding to silica (*A*) and mica (*B*). From this comparison

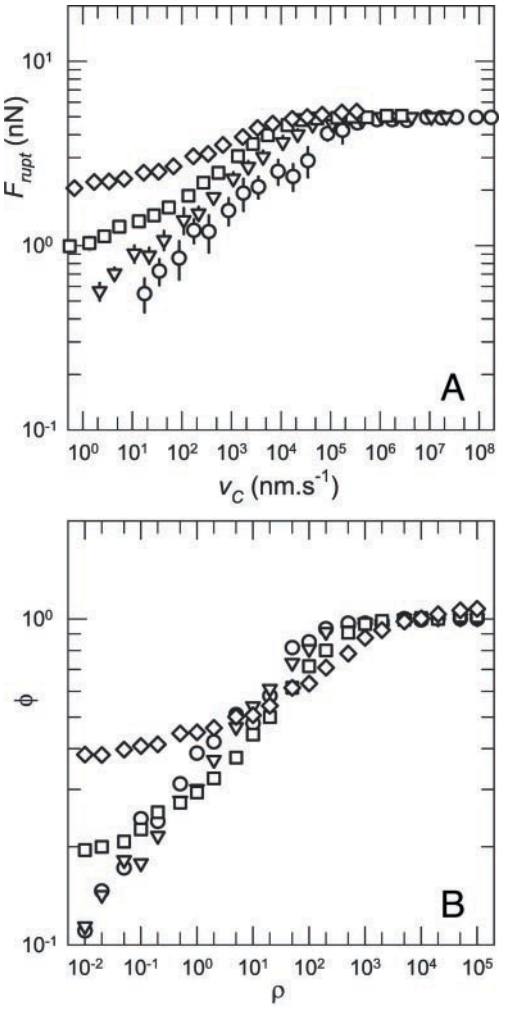

FIGURE 11 (*A*) Rupture force predicted by the multi-bead-and-spring model as a function of the pulling velocity. The four sets of data correspond to the same ratio $n(u_0/k_BT)/r_0 = 500\ \text{nm}^{-1}$ with $u_0 = 10\ k_BT$ at $T = 300$ K, the same diffusivity $D = 10^{-19}\ \text{m}^2\ \text{s}^{-1}$, the same spring stiffness $k = 3\ \text{N m}^{-1}$ and the same cantilever stiffness $k_C = 0.03\ \text{N m}^{-1}$. They differ by the number of bonds n and the potential energy range r_0: $n = 1$ and $r_0 =$ 0.02 nm (*disks*), $n = 2$ and $r_0 = 0.04$ nm (*triangles*), $n = 4$ and $r_0 = 0.08$ nm (*squares*), $n = 8$ and $r_0 = 0.16$ nm (*diamonds*). Each data point represents the average over 10 cycles, and the error bars represent twice the standard error on the mean. (*B*) Representation of the data in *a* using the reduced variables. Especially at low values of ρ it appears that the four sets of forces do not fall on a unique curve.

it follows that, if a range of the potential energy well on the order of 0.1 nm ought to be attained, 4 to 8 springs should be used to represent the molecule, provided that these springs are soft with respect to the cantilever (0.0003 and $0.03\ \text{N m}^{-1}$, respectively, in the present work). It may be emphasized that we end up finally with several fairly well estimated parameters. Indeed, with the sole condition on r_0 not to be too small, we have been able to narrow, step by step, the domain in which the various parameters must be located in order for the model to lead to a satisfactory

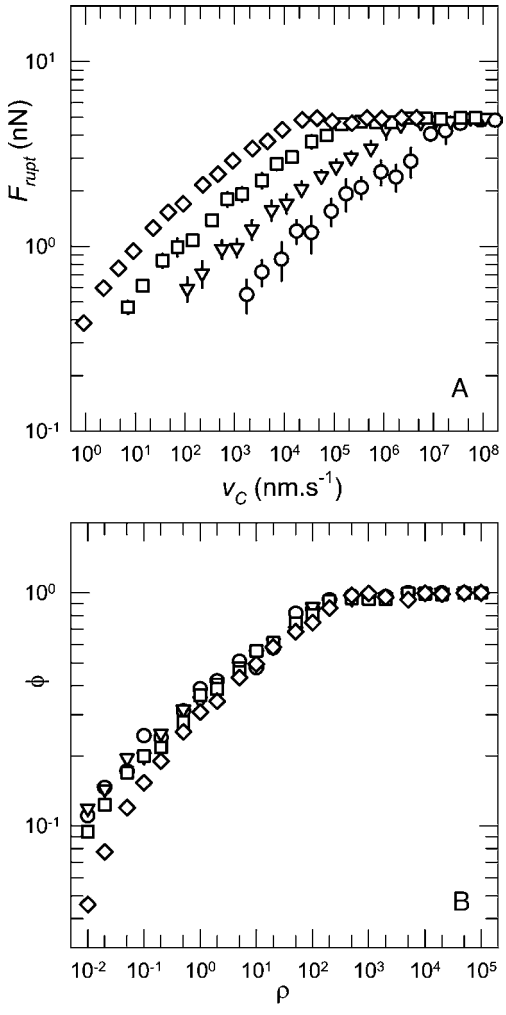

FIGURE 12 Same as Fig. 11, except that $k = 0.0003$ N m^{-1}. Note in particular the change in shape (compare with Fig. 11) of the force curve represented by diamonds induced by the variation of k from 3 to 0.0003 N m^{-1}. (*B*) Representation of the data in *A* using the reduced variables. In contrast to Fig. 11 *B*, it appears that all sets of forces do much better fall on a unique curve.

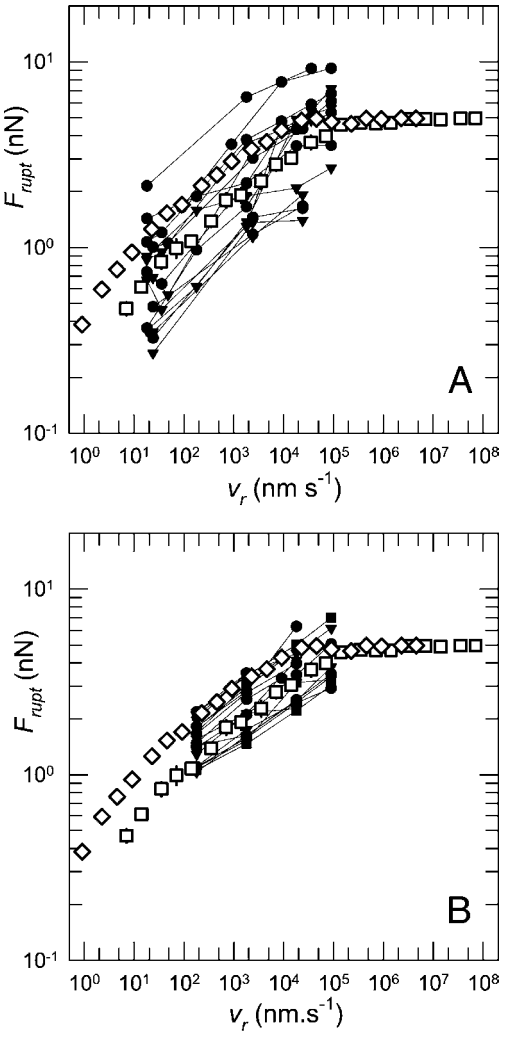

FIGURE 13 Comparison of simulated force curves ($n = 4$, *open squares*; $n = 8$, *open diamonds*), taken from Fig. 12, with the experimental data from Fig. 3 (*closed symbols* connected by *thin lines*). (*A*) Silica surface; (*B*) mica surface.

reproduction of the experimental data. It is also noticeable that the same parameters are suited for both the silica and mica results. It follows that the fibrinogen seems to behave roughly in the same way when it is brought into contact with these surfaces.

As a last point, we may be interested in the possibility to compare the rupture forces corresponding to the multi-bead-and-spring model to those based on Bell's hypothesis (Bell, 1978) where the molecule is assumed to interact with the surface through a single bond whose rupture frequency increases exponentially with the force f applied to it:

$$v = v_0 \exp\left(\frac{f}{f_0}\right) \tag{12}$$

In this expression v_0 corresponds to the off rate at $f = 0$ and f_0 is a characteristic force of the bond, namely the thermal energy divided by the energy barrier width assumed to be independent of f. Using this relationship, we showed that the mean rupture force follows a more complicated law than the logarithmic law valid for the most probable force, given by (Gergely et al., 2000):

$$F_{\text{rupt}} = f_0 \exp\left(\frac{v_0 f_0}{\tilde{R}_{\text{f}}}\right) E_1\left(\frac{v_0 f_0}{\tilde{R}_{\text{f}}}\right) \tag{13}$$

in which E_1 is the exponential integral. The free parameters v_0 and f_0 have been adjusted here so that F_{rupt} based on Bell's hypothesis (Eq. 13) fits optimally the simulated curve corresponding to the multi-bead-and-spring model with $n = 8$, $k = 0.0003$ N m^{-1}, and $k_{\text{C}} = 0.03$ N m^{-1} (open

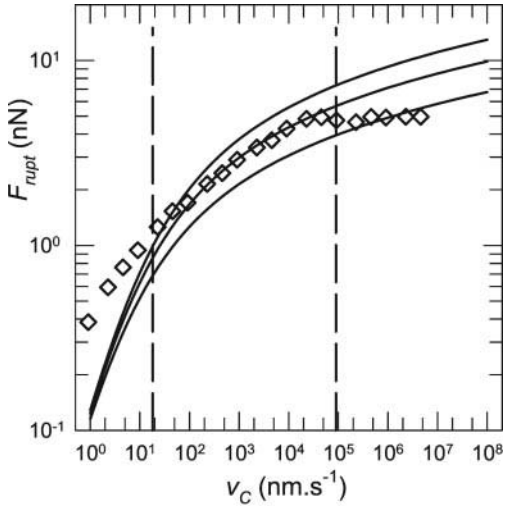

FIGURE 14 Rupture force based on Bell's hypothesis of an exponential dependence of the rupture frequency with respect to the applied force (*lines*), as a function of the pulling velocity. The three lines correspond to $v_0 = 0.01\ s^{-1}$ and $f_0 = 0.4, 0.6, 0.8$ nN (from bottom to top). The simulated data (*diamonds*) are taken from Fig. 12 *A*. The vertical dashed lines delimitate the domain investigated in the fibrinogen/silica experiments.

diamonds in Fig. 13), for v_C ranging from 1 up to 10^8 nm s^{-1}. It appears in Fig. 14 that this is achieved for $v_0 \approx 0.1\ s^{-1}$ and $f_0 \approx 0.6$ nN. As can be seen, the rupture force deduced from Bell's hypothesis can be made to agree reasonably well with the multi-bead-and-spring model prediction on a limited velocity interval. This explains why our experimental results for fibrinogen on silica appeared, in a previous publication (Gergely et al., 2000), to be compatible with a Bell-like approach. If the experiment could have been extended over a few additional orders of magnitude in retraction velocity, it is likely that the weakness of the exponential law would have been revealed. However, even though relation 12 was strictly correct for the rupture of a single bond, the validity of using Eq. 13 in the present context of a multi-bond system would be highly questionable. As a consequence, it seems to be careful not to over-interpret the significance of the two free parameters v_0 and f_0.

SUMMARY AND CONCLUDING REMARKS

We have developed a model aimed to describe the detachment of molecules or cells under a typical AFM force spectroscopy experiment. This model should, however, also constitute a first approach to describe the detachment of cells as a function of the retraction velocity. We have then applied our model to the description of the detachment of fibrinogen molecules adsorbed on silica or mica surfaces as an illustration of the use of our model.

A cell or a protein can interact with a surface through multiple contact points. In our model each contact point is represented by a bead fixed to a spring. All the springs are connected to a common point that is itself connected to a spring representing the AFM cantilever. Each bead is also under the influence of a potential well representing the interaction with the surface. In our model, all the springs associated with the beads and all the potentials are similar. The potentials were taken as 12-6 Lennard-Jones potentials. The displacement of each bead was assumed to be a diffusion process, which was obtained by solving a Langevin equation. Several parameters enter into such a model: the number n of springs, their stiffness k, the stiffness k_C of the spring representing the cantilever, the coefficient D characterizing the diffusion process of the beads and representing the internal dynamics of the protein, finally the parameters u_0 and r_0 defining the Lennard-Jones potential. These latter parameters impose thus also the maximal force that the potential well can oppose to the detachment of a bead in the absence of an external force.

As a general feature, our model predicts, as it is observed experimentally, that whatever the value of the number of interaction points, the rupture force measured in an AFM force experiment is an increasing function of the retraction velocity v_C. We find that at high retraction velocity the rupture forces stay almost constant and equal to n times the maximum force corresponding to the Lennard-Jones potential. In this plateau regime the system behaves in a fully deterministic way, i.e., the thermal fluctuations no longer participate in the detachment process. When the retraction velocity is reduced these thermal fluctuations take an increasing importance in the detachment process. One observes that for a system that interacts with the surface through one point ($n = 1$) the behavior is qualitatively the same whatever the stiffness k of the spring. More precisely, the evolution of the rupture force F_{rupt} as a function of the retraction velocity v_C for a soft spring can be deduced from that corresponding to a hard spring by simply changing the diffusion coefficient. In contrast, as soon as $n > 1$ this scaling law breaks down. Whereas for soft springs the rupture forces evolve qualitatively with v_C in a similar way than for $n = 1$, this is no longer the case for hard "molecular" springs. In this latter case, for $n = 8$ (the highest number of springs that was investigated) the rupture force is much less sensitive to the influence of the retraction velocity than for $n = 1$. This finding suggests that an increase of the number of bonds leads to a macroscopic-like behavior characterized by the independence of F_{rupt} with v_C. In the case of soft springs such a transition to a macroscopic behavior takes also place but it is now the extension of the plateau toward small retraction velocities, which reveals this evolution. Finally, one can also point out that, in the case of one spring or in the case of more than one but soft springs, all the rupture curves "$\ln(F_{rupt})$ vs. $\ln(v_C)$" can reasonably well be mapped on a universal curve "$\ln(\phi)$ vs. $\ln(\rho)$" in which ρ represents a reduced retraction velocity and ϕ a reduced rupture force, both quantities having been defined previously. When applied to analyze the detachment of

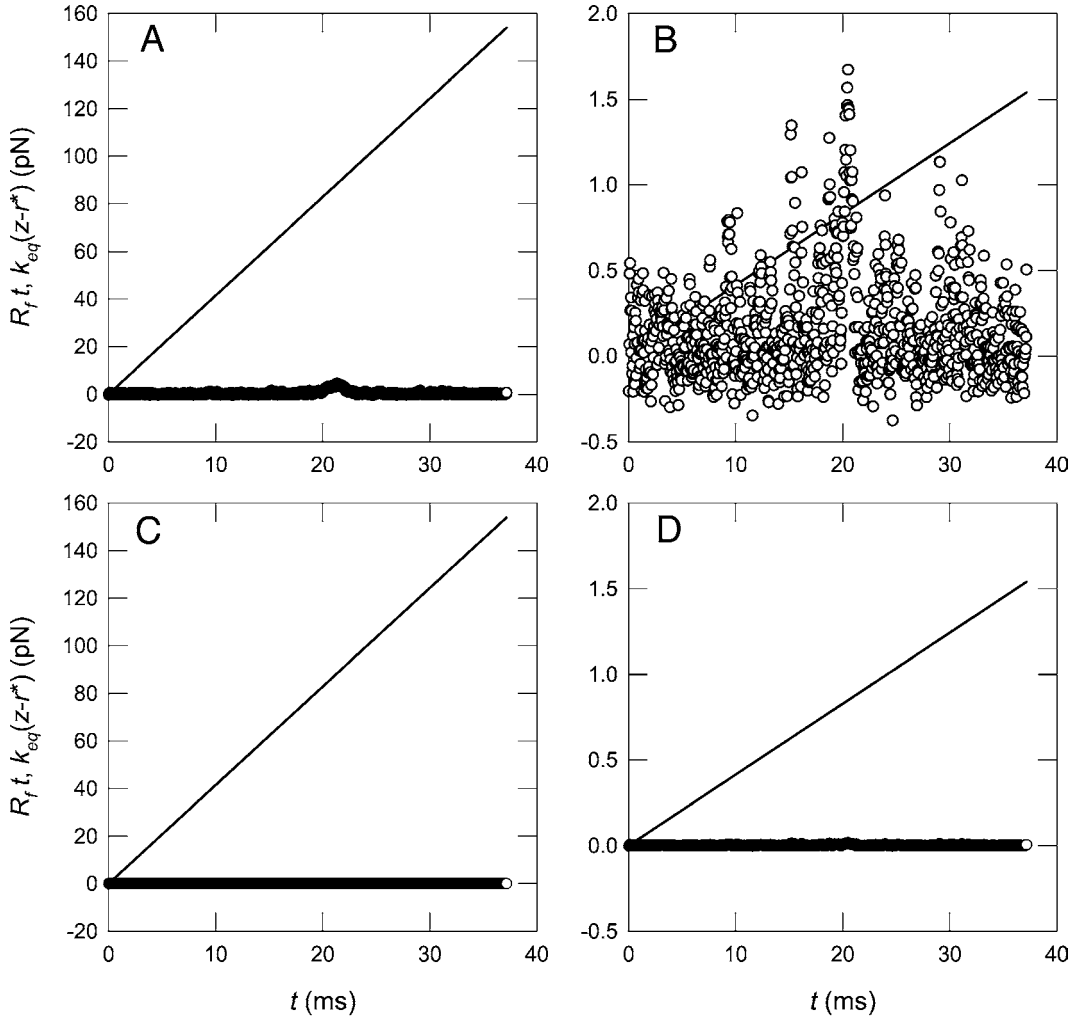

FIGURE 15 Comparison of the opposite of the random component $k_{eq}(z - r^*)$ (*disks*) and the deterministic component $R_f t$ (*straight line*) of the pulling force as a function of time. Five millions of steps have been simulated, but only 1 point on 5000 is represented for the sake of clarity. Common parameters: $n = 1$, $u_0 = 5\ k_B T$ at $T = 300$ K, $r_0 = 0.1$ nm, $k_C = 0.03$ N m^{-1}, $D = 10^{-18}\ m^2\ s^{-1}$. (*A*) $\rho = 1$ and $k = 3$ N m^{-1}, (*B*) $\rho = 10^{-2}$ and $k = 3$ N m^{-1}, (*C*) $\rho = 1$ and $k = 0.0003$ N m^{-1}, (*D*) $\rho = 10^{-2}$ and $k = 0.0003$ N m^{-1}.

fibrinogen from a solid surface measured by AFM force spectroscopy, we found that the one bead-and-spring model is not able to account for the measured data. A reasonable good agreement is found with an 8-bead-and-spring model whose springs are soft compared with the cantilever.

APPENDIX

We give in this Appendix a rational basis to the definition of the reduced retraction rate ρ (Eq. 11), at least in the particular case of a 1-bead-and-spring system. To this end we start from Eq. 7 and define the dimensionless distance ζ by z/r_0 and the dimensionless time τ by Dt/r_0^2. Accordingly, this equation is rewritten as:

$$\Delta\zeta = \frac{Fr_0}{k_B T}\Delta\tau + g_z\sqrt{2\Delta\tau} \tag{A1}$$

in which the index i has been omitted to simplify the notation, and g_z is a normal random variable of mean equal to zero and variance equal to unity. The force F consists of two contributions, the LJ force and the spring force, i.e., $F = F_{LJ} + f$, in which:

$$F_{LJ} = 48\,\frac{u_0}{r_0}\left[\left(\frac{r_0}{z}\right)^{13} - \frac{1}{2}\left(\frac{r_0}{z}\right)^{7}\right] \tag{A2a}$$

$$f = k(z_B - z - \ell_0) \tag{A2b}$$

This formulation is, however, not convenient for our purpose, because z_B, being a function of z, is itself fluctuating and therefore cannot be expressed as a simple function of t. In contrast, if we express the pulling force exerted on the particle using z_C instead of z_B, and write the strictly equivalent relation $f = k_{eq}(z_C - z - 2\ell_0)$, we can use $z_C = v_C t + r^* - 2\ell_0$, which is purely deterministic. Thus:

$$f = k_{eq}(v_C t + r^* - z) = R_f t - k_{eq}(z - r^*) \tag{A2c}$$

Again, using the dimensionless variables ζ and τ, F_{LJ} and f can be rewritten as:

$$F_{LJ} = 48\,\frac{u_0}{r_0}\left(\frac{1}{\zeta^{13}} - \frac{1}{2\zeta^{7}}\right) \tag{A3a}$$

$$f = k_{eq}\left[v_C\,\frac{r_0^2\tau}{D} - r_0\left(\zeta - \frac{r^*}{r_0}\right)\right] \tag{A3b}$$

Using Eq. 3 with $n = 1$, i.e., $K = k$, it follows that:

$$\frac{Fr_0}{k_BT} = 48\,\frac{u_0}{k_BT}\,h(\zeta) + R_f\,\frac{r_0^3}{Dk_BT}\,\tau - \frac{k_{eq}r_0^2}{k_BT}\left(\zeta - \frac{r^*}{r_0}\right) \tag{A4}$$

in which $h(\zeta) = 1/\zeta^{13} - 1/2\zeta^{7}$. One gets then finally:

$$\Delta\zeta = \left[48\,\frac{u_0}{k_BT}\,h(\zeta) + \rho\tau - \frac{k_{eq}r_0^2}{k_BT}\left(\zeta - \frac{r^*}{r_0}\right)\right]\Delta\tau + g_z\sqrt{2\Delta\tau} \tag{A5}$$

in which $\rho = kk_Cv_Cr_0^3/(k + k_C)Dk_BT$. *If* $n > 1$, k must be replaced by $K = nk$. If the detachment occurs within a sufficiently short time, z is hardly different from its initial value r^*. Then, the applied force f is quasi-deterministic and is given to a high degree of accuracy by $f = R_f t$ as shown by Eq. A2c. This explains that the parameter combination defining the reduced loading rate ρ can serve as a common variable for different simulations as in Fig. 5. In these circumstances, we see also that several combinations of the system parameters can lead to the same value of ρ and hence are indistinguishable.

To illustrate the importance of the third term in the square bracket of Eq. A5, we give in Fig. 15 *A* and *B* a comparison between two simulations using the parameters $u_0 = 5\ k_BT$ at $T = 300$ K, $r_0 = 0.1$ nm, $k_C = 0.03$ N m^{-1}, $k = 3$ N m^{-1}, $D = 10^{-18}$ m^2 s^{-1}, but differing by the value of ρ, hence of v_C. As can be seen, at $\rho = 1$, the random component $-k_{eq}(z - r^*)$ of f is very small with respect to the deterministic component $R_f t$ after a small initial period of time (Fig. 15 *A*). In contrast, at $\rho = 10^{-2}$, the force induced by the thermal noise is considerably larger if compared with $R_f t$ (Fig. 15 *B*). In this case the loading rate is in fact not constant even though point *C* moves at constant velocity. These simulations have been repeated with $k = 0.0003$ N m^{-1} (Fig. 15 *C* and *D*). The evolution when ρ decreases (from Fig. 15 *C* to *D*) is qualitatively the same (a magnification would help to see that the fluctuations are indeed the largest at the smallest loading rate). Nonetheless, it can be observed that in both cases the noise is very weak if compared with the controlled component $R_f t$.

It follows from the above discussion that at the slow retraction velocity corresponding to $\rho = 10^{-2}$ and $k = 3$ N m^{-1}, the variable ρ cannot alone account for the development of the process, and the scaling breaks down. As was seen in Fig. 5 *B*, at $\rho = 1$ the simulation results coincide whether they correspond to $k = 3$ or 0.0003 N m^{-1}, whereas at $\rho = 10^{-2}$ the predicted rupture force depends not only on ρ but also on k itself (compare the closed triangle with the closed disk at this loading rate).

Note in closing this appendix that for systems with two or more springs, the theoretical analysis is much more complicated because of the coupling of all particles. This is due to the fact that the loading rate on one particle depends on the position of the bar *B* whose position, in turn, depends on all particle positions (see Eq. 10). Because the position of *B* is the most sensitive to the particle positions when k is large, the coupling is also the strongest when k is large.

The authors are indebted to Professor Robijn Bruinsma for interesting discussions. Part of the work was supported by the contract APEX 99-13 from the Institut National de la Santé et de la Recherche Médicale, and the "Action Concerteé Incitative-Surfaces, Interfaces et Conception de Nouveaux Matèriaux" (2001) from the Ministère de la Recherche.

REFERENCES

Bell, G. I. 1978. Models for the specific adhesion to cells. *Science.* 200:618–627.

Benoit, M., D. Gabriela, G. Gerisch, and H. E. Gaub. 2000. Discrete interactions in cell adhesion measured by single-molecule force spectroscopy. *Nat. Cell Biol.* 2:313–317.

Bongrand, P. 1994. Adhesion of cells. *In* Handbook of Physics of Biological Systems, Vol. 1. R. Lipowsky, editor. Elsevier Science BV, Amsterdam. 729–773.

Bowen, W. R., N. Hilal, R. W. Lovitt, and C. J. Wright. 1998. Direct measurement of interactions between adsorbed protein layers using an atomic force microscope. *J. Colloid Interface Sci.* 197:348–352.

Dammer, U., M. Hegner, D. Anselmetti, P. Wagner, M. Dreier, W. Huber, and H.-J. Güntherodt. 1996. Specific antigen/antibody interactions measured by force microscopy. *Biophys. J.* 70:2437–2441.

Dufrêne, Y. F., C. J. P. Boonaert, P. A. Gerin, M. Asther, and P. G. Rouxhet. 1999. Direct probing of the surface ultrastructure and molecular interactions of dormant and germinating spores of *Phanerochaete chrysosporium*. *J. Bacteriol.* 181:5350–5354.

Eckert, R., S. Jeney, and J. K. H. Hörber. 1997. Understanding intercellular interactions and cell adhesion: lessons from studies on protein-metal interactions. *Cell Biol. Int.* 21:707–713.

Ermak, D. L., and J. A. McCammon. 1978. Brownian dynamics with hydrodynamic interactions. *J. Chem. Phys.* 69:1352–1360.

Evans, E. 1998. Energy landscapes of biomolecular adhesion and receptor anchoring at interfaces explored with dynamic force spectroscopy. *Faraday Discuss.* 111:1–16.

Evans, E. 1999. Looking inside molecular bonds at biological interfaces with dynamic force spectroscopy. *Biophys. Chem.* 82:83–97.

Evans, E., and F. Ludwig. 2000. Dynamic strengths of molecular anchoring and material cohesion in fluid membranes. *J. Phys. Condens. Matter.* 12:A315–A320.

Evans, E., and K. Ritchie. 1997. Dynamic strength of molecular adhesion bonds. *Biophys. J.* 72:1541–1555.

Evans, E., and K. Ritchie. 1999. Strength of a weak bond connecting flexible polymer chains. *Biophys. J.* 76:2439–2447.

Fisher, T. E., A. F. Oberhauser, M. Carrion-Vazquez, P. E. Marszalek, and J. M. Fernandez. 1999. The study of protein mechanics with the atomic force microscope. *Trends Biochem. Sci.* 24:379–384.

Florin, E.-L., M. Rief, H. Lehmann, M. Ludwig, C. Dornmair, V. T. Moy, and H. E. Gaub. 1995. Sensing specific molecular interactions with the atomic force microscope. *Biosens. Bioelectron.* 10:895–901.

Fritz, J., A. G. Katopodis, F. Kolbinger, and D. Anselmetti. 1998. Force-mediated kinetics of single P-selectin/ligand complexes observed by atomic force microscopy. *Proc. Natl. Acad. Sci. U.S.A.* 95:12283–12288.

Gergely, C., B. Senger, J.-C. Voegel, J. K. H. Hörber, P. Schaaf, and J. Hemmerlé. 2001. Semi-automatized processing of AFM force-spectroscopy data. *Ultramicroscopy.* 87:67–78.

Gergely, C., J.-C. Voegel, P. Schaaf, B. Senger, M. Maaloum, J. K. H. Hörber, and J. Hemmerlé. 2000. Unbinding process of adsorbed proteins under external stress studied by AFM force spectroscopy. *Proc. Natl. Acad. Sci. U.S.A.* 97:10802–10807.

Hemmerlé, J., S. M. Altmann, M. Maaloum, J. K. H. Hörber, L. Heinrich, J.-C. Voegel, and P. Schaaf. 1999. Direct observation of the anchoring process during the adsorption of fibrinogen on a solid surface by force-spectroscopy mode atomic force microscopy. *Proc. Natl. Acad. Sci. U.S.A.* 96:6705–6710.

Hinterdorfer, P., W. Baumgartner, H. J. Gruber, K. Schilcher, and H. Schindler. 1996. Detection and localization of individual antibody-antigen recognition events by atomic force microscopy. *Proc. Natl. Acad. Sci. U.S.A.* 93:3477–3481.

Hinterdorfer, P., K. Schilcher, W. Baumgartner, H. J. Gruber, and H. Schindler. 1998. A mechanistic study of the dissociation of individual

antibody-antigen pairs by atomic force microscopy. *Nanobiology.* 4:177–188.

Hoh, J. H., J. P. Cleveland, C. B. Prater, J.-P. Revel, and P. K. Hansma. 1992. Quantized adhesion detected with the atomic force microscope. *Am. Chem. Soc.* 114:4917–4918.

Izrailev, S., S. Stepaniants, M. Balsera, Y. Oono, and K. Schulten. 1997. Molecular dynamics study of unbinding of the avidin-biotin complex. *Biophys. J.* 72:1568–1581.

Lo, Y.-S., N. D. Huefner, W. S. Chan, F. Stevens, J. M. Harris, and T. P. Beebe, Jr. 1999. Specific interactions between biotin and avidin studied by atomic force microscopy using the Poisson statistical analysis method. *Langmuir.* 15:1373–1382.

Mège, J.-L., C. Capo, A.-M. Benoliel, and P. Bongrand. 1986. Determination of binding strength and kinetics of binding initiation. *Cell Biophys.* 8:141–160.

Merkel, R., P. Nassoy, A. Leung, K. Ritchie, and E. Evans. 1999. Energy landscapes of receptor-ligand bonds explored with dynamic force spectroscopy. *Nature.* 397:50–53.

Moy, T., E. L. Florin, and H. E. Gaub. 1994. Intermolecular forces and energies between ligands and receptors. *Science.* 266:257–259.

Rief, M., J. Pascual, M. Saraste, and H. E. Gaub. 1999. Single molecule force spectroscopy of spectrin repeats: low unfolding forces in helix bundles. *J. Mol. Biol.* 286:553–561.

Ritchie, K. 1998. Probing nanoscale adhesion and structure at soft interfaces. PhD Thesis, The University of British Columbia, Vancouver.

Seifert, U. 2000. Rupture of multiple parallel molecular bonds under dynamic loading. *Phys. Rev. Lett.* 84:2750–2753.

Strigl, M., D. A. Simson, C. M. Kacher, and R. Merkel. 1999. Force-induced dissociation of single protein A-IgG bonds. *Langmuir.* 15: 7316–7324.

Strunz, T., K. Oroszlan, R. Schäfer, and H.-J. Güntherodt. 1999. Dynamic force spectroscopy of single DNA molecules. *Proc. Natl. Acad. Sci. U.S.A.* 96:11277–11282.

Strunz, T., K. Oroszlan, I. Schumakovitch, H.-J. Güntherodt, and M. Hegner. 2000. Model energy landscapes and the force-induced dissociation of ligand-receptor bonds. *Biophys. J.* 79:1206–1212.

van Kooten, T. G., J. M. Schakenraad, H. C. van der Mei, and H. J. Busscher. 1992. Influence of substratum wettability on the strength of adhesion of human fibroblasts. *Biomaterials.* 13:897–904.

Willemsen, O. H., M. M. E. Snel, K. O. van der Werf, B. G. de Grooth, J. Greve, P. Hinterdorfer, H. J. Gruber, H. Schindler, Y. van Kooyk, and C. G. Figdor. 1998. Simultaneous height and adhesion imaging of antibody-antigen interactions by atomic force microscopy. *Biophys. J.* 75:2220–2228.